Article

Development of Broadband Resistive–Capacitive Parallel–Connection Voltage Divider for Transient Voltage Monitoring

Shijun Xie [1,*], Zhou Mu [1], Weidong Ding [2], Zhenbo Wan [2], Shaochun Su [3], Chenmeng Zhang [1], Yu Zhang [1], Yalong Xia [1] and Donghui Luo [1]

[1] State Grid Sichuan Electric Power Research Institute, Chengdu 610041, China; mu_zhou@126.com (Z.M.); zcm@whu.edu.cn (C.Z.); dkybyz@foxmail.com (Y.Z.); cdxyl@foxmail.com (Y.X.); l_dh@cqu.edu.cn (D.L.)
[2] School of Electrical Engineering, Xi'an Jiaotong University, Xi'an 710049, China; wdding@xjtu.edu.cn (W.D.); claisen@stu.xjtu.edu.cn (Z.W.)
[3] State Grid Sichuan Electric Power Company, Chengdu 610041, China; susc8452@sc.sgcc.com.cn
[*] Correspondence: xieshijun@tsinghua.org.cn; Tel.: +86-286-999-5134

Abstract: The on-site measurement of transient voltages is of great significance in analyzing the fault cause of power systems and optimizing the insulation coordination of power equipment. Conventional voltage transformers normally have a narrow bandwidth and are unable to accurately measure various transient voltages in power systems. In this paper, a wideband parallel resistive–capacitive voltage divider is developed, which can be used for online monitoring of transient voltages in a 220 kV power grid. The structures of the high-voltage and low-voltage arms were designed. The internal electric field distribution of the high-voltage arm was analyzed. The influence factors and improvement techniques of the upper frequency limit were studied. The parameters of the elements of the divider were determined. The voltage withstand performances and scale factors under lightning impulses and AC and DC voltages, the temperature stabilities of scale factors and the step response and bandwidth of the developed voltage divider were tested. The results show that the deviations of the scale factors under various voltage waveforms and different temperatures ranging from −20 to 40 °C are within 3%. The withstand voltage meets the relevant requirements specified in IEC60071-1-2011. The step response 10~90% rise time is approximately 29 ns, and the 3 dB bandwidth covers the range of DC to 10 MHz.

1. Introduction

Precise measurement of transient voltage waveforms in power systems is of great significance to fault analysis, optimal insulation design, optimized high-voltage experiments, etc. At present, online monitoring of transient voltages can be achieved by a voltage transformer, bushing tap, optical electric field sensor, high-voltage divider, etc. [1–5]. Among them, voltage transformers are made of a non-linear ferromagnetic material and have a narrow bandwidth [6–9]. Optical electric field sensors have a good performance in terms of bandwidth, but their practical measurement accuracy is limited by their poor stability against temperature, vulnerability to vibration and inter-phase coupling [10]. The application of the bushing tap method interrupts the grounding connection of the tap, which introduces a safety risk [11]. Therefore, a broadband high-voltage divider is required, to a certain extent, in power systems for transient voltage monitoring.

Intensive studies have been carried out on voltage dividers globally. The basic types of voltage divider include capacitive and resistive dividers. A capacitive voltage divider using a gas capacitor for the high-voltage arm and a mica dielectric for the low-voltage arm has a

step response time of less than 20 ns and a good measurement of standard impulse wave-forms [12]. A commonly used coaxial configuration for capacitive voltage dividers was developed by Standford in the 1960s, which demonstrates good temperature stability [13]. High-precision resistive voltage dividers commonly use metallic film resistors arranged in a coaxial chamber and have a step response time of less than 1 ns [14–16]. Liquid resistors can also be used in a resistive divider for heat dissipation and limiting stray parameters, which provides a 13 ns response time, as reported by Liu Y. [17]. Capacitive–resistive combined dividers are more likely to be used in practical applications. The parallel-connected resistive–capacitive voltage divider developed by T. Harada has a step response time of about 10 ns [18]. Sweden developed an HVDC voltage divider based on RC compound connection, which has an uncertainty of 16×10^{-6} in DC measurement [19]. Kai Zhou developed a low-damped capacitive voltage divider for online transient monitoring of a 10 kV distribution network. By appropriately determining the damping resistance, high-voltage arm capacitance and other parameters, a minimized oscillation and good impulse response were achieved with the divider [20]. A non-contact measurement can be achieved by voltage division via space capacitance. A non-contact voltage division technique was developed by hanging a sensor on a high-voltage conductor, which showed a similar performance to capacitive voltage dividers [21]. In non-contact voltage division, the sensing electrode is more likely to be installed on the ground, in which the space capacitance between the conductor and sensing electrode is used as a high-voltage arm [22,23]. These non-contact voltage division techniques have the advantages of a low cost and easy application, although the inter-phase coupling issue reduces their practicality. Voltage division is also applied in gas-insulated switchgear (GIS) to measure VFTO caused by the switching operation. Similar to non-contact voltage division, space capacitance between the conductor and installed electrode is used as a high-voltage arm. Based on cone-shape design of the low-voltage arm, H. Murase developed a GIS sensor with a step response time of 350 ps and an upper frequency limit beyond 1 GHz [24]. However, the measuring point of this technique is limited to GIS. Overall, although the above voltage division techniques are characterized by a short response time, most of them only function sufficiently in laboratory environments and low-voltage measurement. Some are not enabled with low-frequency measurement (i.e., harmonics), and some are vulnerable to the adjacent equipment and the temperature. The increase in the voltage level would enlarge the physical size of the divider, thus introducing more stray parameters and worsening the response. Therefore, it is a challenge to use a divider to perform on-site measurement of transients. In addition, insulation of the outdoor environment as well as the temperature stability must be within acknowledged limits for the divider.

In this paper, a parallel-connected resistive–capacitive voltage divider is developed for a 220 kV power grid. The development works include the structural design of high and low arms, analysis of the internal field distribution, a study on the upper cut-off frequency of the divider and its optimization and the determination of the components' parameters. In verifying the divider's performance, the insulation strength and scale factors were determined by a lightning impulse, the power frequency and the DC voltage. The temperature stability was tested in an artificial climate chamber. The response characteristics of the divider were tested by the step response method and frequency sweep method.

2. Structural Design

2.1. High-Voltage Arm

In order to meet the demand of monitoring various transients in the outdoor environment, the divider developed in this paper is characterized by good resistance against the environment, high temperature stability and a strong broadband measurement. The porcelain housing of a 252 kV specification was used to pack the divider. The divider was equipped with components with high temperature stability. To achieve a low-frequency measurement (i.e., DC to harmonics), a parallel connection of resistance and capacitance was adopted. Meanwhile, for a better high-frequency performance, minimization of high-voltage arm

inductance and a properly damped design were adopted. Fine adjustment was performed on the resistance and capacitance values for both the high- and low-voltage arms.

The schematic diagram of the voltage divider is shown in Figure 1. A total of 25 units were assembled in series connection in the high-voltage arm to reduce the insulation requirement for a single component. In each unit in the high-voltage arm, C is the capacitance, and R_d denotes the damping resistance. R is the parallel-connected resistance, and C_{g-n} is the stray capacitance to the ground of each unit. A resistive–capacitive parallel connection was also adopted in the low-voltage arm, in which c is the capacitor, r_d is the compensation resistor and r is the parallel-connected resistor. C_g denotes the stray capacitance to the ground of the low-voltage arm. The capacitors work on the division of high-frequency voltage waveforms, while the parallel-connected resistors are for the low-frequency voltage, even including DC. The damping resistance and compensation resistance damp the high-frequency oscillation and manage the scale factor at high frequencies.
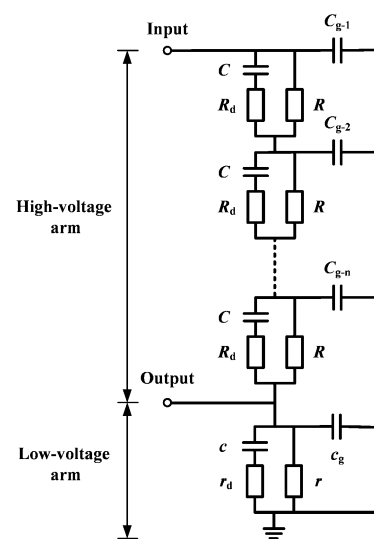
Figure 1. Circuit structure of resistive–capacitive voltage divider.

Conventional parallel-connected resistive–capacitive voltage dividers are mainly used for DC and power frequency measurements, of which the high-frequency performance is generally not sufficiently developed. A large physical size is generally required for the sake of the insulation strength consideration, which limits the high-frequency performance by introducing stray parameters (i.e., stray capacitance and lead inductance). In order to reduce the lead inductance, each unit in the high-voltage arm includes a parallel connection of five groups of capacitors and damping resistors. In order to improve the thermal capacity of the parallel resistances, each unit has five resistors in parallel, as shown in Figure 2. The height of each unit is only 80 mm.
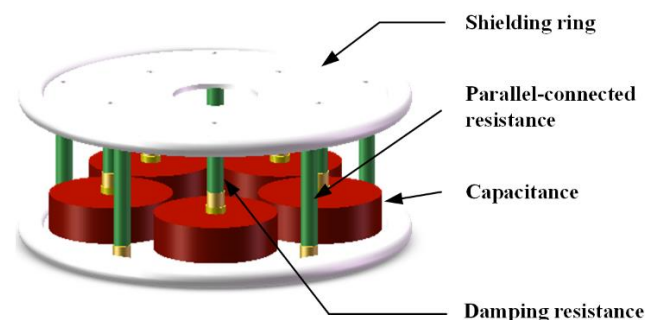
Figure 2. Structure of the high-voltage unit.

Meanwhile, in order to ensure the temperature stability of the voltage divider, a temperature-compensated (negative–positive 0 ppm/°C) ceramic capacitor with stable capacitance and dielectric loss and a glass glaze resistor with a small temperature coefficient were used in the high-voltage arm [25].

To even out the electric field distribution and prevent partial discharge, an aluminum shielding electrode with a shielding ring was arranged between adjacent units, which also reinforces the mechanical strength of the high-voltage arm.

A total of 25 high-voltage arm units were divided into 5 groups, which were installed in series on an insulating pillar. The whole high-voltage arm was installed in a 252 kV porcelain casing with a height of 2.3 m. The top of the casing was equipped with a shielding ring. The casing was filled with transformer oil as insulation and a cooling medium.

2.2. Field Distribution in the High-Voltage Arm

In order to avoid the internal discharge of the voltage divider, the internal electric field distribution of the designed high-voltage arm was simulated and analyzed by the finite element method.

An air-type spherical solution domain with a diameter of 5 times the height of the voltage divider was set around the divider with the boundary grounded and the domain tetrahedrally meshed. The basic properties of various materials involved in the simulation computation are shown in Table 1.

Table 1. Electrical property parameters of materials.

Material	Conductivity (S/m)	Relative Dielectric Constant
Parallel-connected resistor	0.002	6
Series-connected resistor	788	6
Capacitor	1×10^{-12}	146
Transformer oil	1×10^{-12}	2.3
Casing	2.01×10^{-15}	6
Stainless-steel components	4.03×10^{6}	1
Insulating pillar	2.01×10^{-15}	6
Spherical solution domain	5×10^{-14}	1

The electric field simulation adopted the Dirichlet boundary condition to solve the problem [26]. The excitation potential was applied on the metal flange at the top the voltage divider, and the metal flange at the bottom of the voltage divider was grounded. The simulation results are shown in Figures 3–5 for when the applied voltage was 360 kV, which is the highest tolerated power frequency voltage. The high-field strength area outside the divider body is mainly distributed at the edge of the top shielding electrode, with the maximum value of 2.40 kV/mm. The highest field strength inside the divider appears at the connection point of the capacitor and resistor in the resistive–capacitive branch, which is 3.49 kV/mm. The breakdown field strength of the transformer oil is no less than 28 kV/mm, which is much higher than the calculated maximum local field strength; thus, internal discharge is not likely to occur under normal operating conditions.
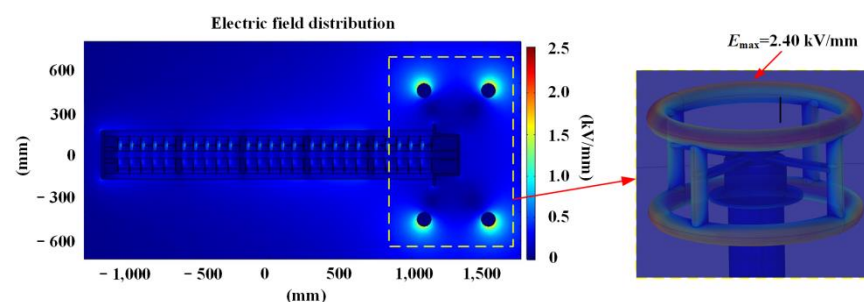
Figure 3. Electric field distribution of the high–voltage arm.

Electric field distribution
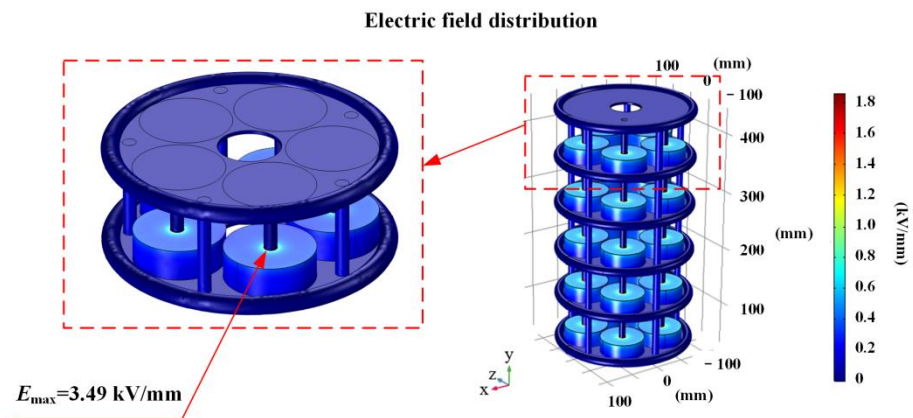
Figure 4. Electric field distribution of the unit in the high–voltage arm.

Electric field distribution
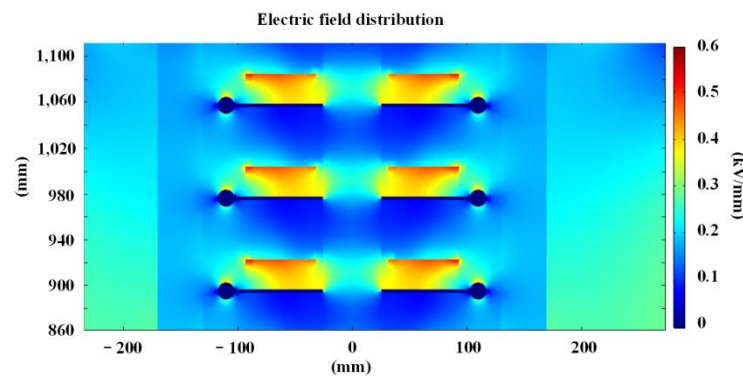
Figure 5. Electric field distribution at the edges of the shielding electrodes.

2.3. Low-Voltage Arm

In order to reduce the stray inductance of the low-voltage arm, multiple groups of resistors and capacitors were placed in parallel in the low-voltage arm, in which the components were compactly welded on a PCB (as shown in Figure 6). A non-inductive symmetrical structure for both sides was adopted for the PCB [27]. In addition, resistor and capacitor chip elements with a small temperature drift and low inductance were used.
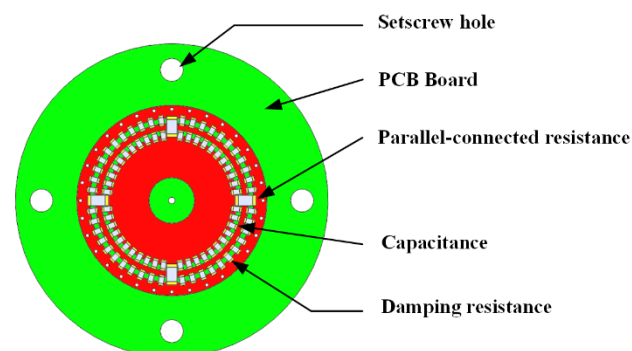
Figure 6. Structure of the low–voltage arm.

3. Frequency Response Analysis

The low-frequency performance of a resistive–capacitive parallel-connected voltage divider is mainly determined by the circuit of parallel resistors. Its upper cut-off frequency is affected by various parameters including lead inductance and stray capacitance. Thus, it is necessary to analyze the influencing factors and optimization methods in detail.

For the high-frequency voltage measurement, the parallel resistors can be ignored, and the equivalent circuit of the voltage divider is shown in Figure 7, where L_0 is the lead inductance introduced by the external lead, and C_0 is the stray capacitance of the divider to the ground. L_1 and L_2 denote the lead inductance of the high- and low-voltage arms, respectively. C_1 and C_2 denote the capacitance for the high- and low-voltage arms, respectively. R_1 is the damping resistance of the high-voltage arm, and R_2 is the compensation resistance of the low-voltage arm. U_1 is the input voltage, and U_0 is the output voltage. The upper cut-off frequency of the voltage divider mainly depends on three groups of LC units, namely, L_0C_0, L_1C_1 and L_2C_2.
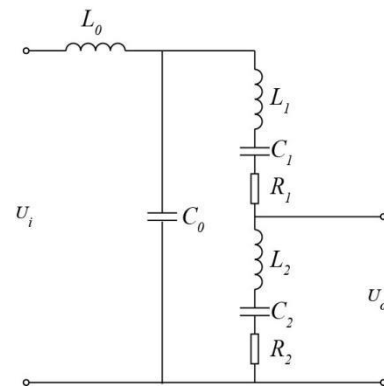
Figure 7. Equivalent circuit of the resistive–capacitive voltage divider during measurement of high-frequency voltage.

The frequency characteristic in the amplitude of the voltage divider via the frequency sweeping method is shown in Figure 8 for when $L_0C_0 \gg L_1C_1$ and L_2C_2. The calculation shows that, when the measured frequency is close to the resonance point of L_0C_0, the output voltage increases by several times that of the flat section. With the further increase in frequency, reactance L_0 gradually exceeds reactance C_0, the voltage divided by the divider gradually decreases and the output voltage decreases. In this case, the upper cut-off frequency of the voltage divider is mainly determined by the L_0C_0 resonant frequency. The resonant frequency ω_0 of L_0C_0 is

$$\omega_0 = \frac{1}{\sqrt{L_0C_0}} \tag{1}$$
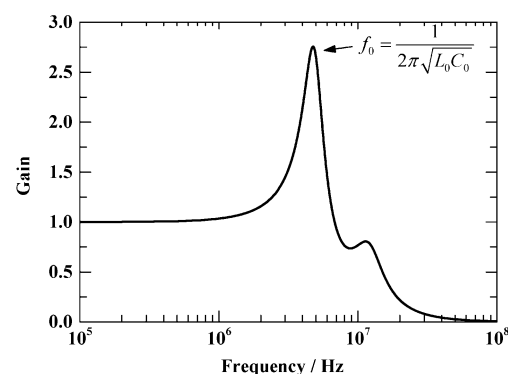
Figure 8. Amplitude–frequency characteristics of the voltage divider when $L_0C_0 \gg L_1C_1$ and L_2C_2.

By reducing the lead inductance L_0 and the stray capacitance C_0 to the ground, the resonant frequency of L_0C_0 can be lifted, which improves the upper cut-off frequency.

In the case where $L_0C_0 << L_1C_1$ and L_2C_2, L_0C_0 can be ignored, and the voltage imposed on the divider is the supplier's voltage. The transfer function of the output signal is

$$h(s) = \frac{L_2s + R_2 + \frac{1}{sC_2}}{Ls + R + \frac{1}{sC}} \tag{2}$$

where

$$R = R_1 + R_2 \tag{3}$$

$$L = L_1 + L_2 \tag{4}$$

$$C = C_1C_2/(C_1 + C_2) \tag{5}$$

According to the above transfer function, the amplitude–frequency characteristic curves of the voltage divider in the cases of $L_1C_1 > L_2C_2$ and $L_1C_1 < L_2C_2$ are shown with the solid line and dotted line in Figure 9, respectively. If $L_1C_1 > L_2C_2$ applies, the upper cut-off frequency of the voltage divider is mainly determined by L_1C_1. Otherwise, the upper cut-off frequency is mainly determined by L_2C_2. Because the scale factor for DC measurement is mainly determined by the ratio of parallel resistance of the high- and low-voltage arms, and the scale factor for the medium frequencies is mainly determined by the reciprocal of the capacitance ratio of the high- and low-voltage arms, the capacitance ratio and the parallel resistance ratio of the high- and low-voltage arms must be kept identical in order to ensure the consistency of the scale factor for DC and medium frequencies. Therefore, the effective measure to improve the upper cut-off frequency is to limit the lead inductance.
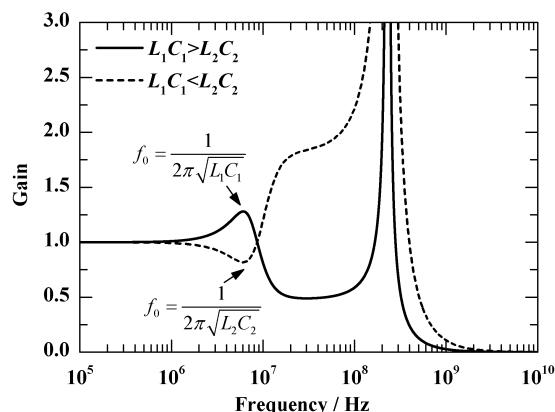
Figure 9. The influence of the resonance points of high– and low–voltage arms on the amplitude–frequency characteristics.

4. Parameter Determination

4.1. High-Voltage Arm Components

On the condition that the maximum amplitude of the measured voltage is assured, considering the insulation strength of the low-voltage arm and the signal-to-noise ratio of the output signal, the scale factor of the voltage divider was preliminarily designed as 10,000:1.

For the low-damped capacitive voltage divider, the damping resistance of the high-voltage arm is supposed to match the wave impedance of the high-voltage lead (about 300 Ω or greater) [28]. In addition, considering the large physical size of the voltage divider, it is difficult to effectively reduce the ground capacitance; thus, the value of damping resistance could be increased accordingly.

The inductance L of the high-voltage arm is estimated by the inductance calculation equation of the cylindrical conductor,

$$L = \frac{\mu_0 l}{2\pi} (\ln \frac{2l}{r} - 0.75) \tag{6}$$

where r is the outer diameter of the high-voltage arm, L is the height of the high-voltage arm and μ_0 is the vacuum permeability. The self-inductance of the high-voltage arm is supposed to be several μH. Taking 10 MHz as the expected upper cut-off frequency, according to Equation (1), the capacitance value of the high-voltage arm is supposed to be tens of pF.

The scale factor transition point of DC to low-frequency voltage is determined by the parallel resistance. A higher resistance causes a lower transition frequency. However, a high-resistance resistor is generally poor in accuracy and stability. Therefore, the resistance of the parallel resistor should be determined by a compromise. In this paper, the power frequency is selected as the transition frequency; thus, by only considering that the capacitive reactance of the high-voltage arm is far less than the parallel resistance, the deviation of the power frequency measurement in the transition section can be further adjusted by the parameters of the low-voltage arm.

Based on the theoretical estimation and actual situation, it is determined that, in the high-voltage arm, a single capacitor has a capacitance of 220 pF, 5 capacitors are connected in parallel to form a single unit of the high-voltage arm and 25 units are connected in series to form the high-voltage arm. Thus, the total capacitance of the high-voltage arm is 44 pF. A single damping resistor has 80 Ω, and the total damping resistance of the high-voltage arm is 400 Ω; a single parallel resistor has 50 MΩ, and the total parallel resistance of the high-voltage arm is 250 MΩ.

4.2. Low-Voltage Arm Components

The parallel resistance and capacitance of the low-voltage arm are determined according to the designed scale factor and determined parameters of the high-voltage arm.

For a conventional resistive–capacitive voltage divider, a pure capacitor branch can generally be found in the low-voltage arm. When the frequency is close to the *LC* resonant frequency of the high- and low-voltage arms, the impedance of the high-voltage arm can be approximated to a damping resistance with hundreds of ohms. The capacitive reactance almost offsets the inductive reactance in the low-voltage arm, and the overall impedance is very low, resulting in an obviously elevated scale factor and weak output signal. Therefore, in order to enable the divider to measure the high-frequency voltage, it is necessary to connect a resistor in series in the low-voltage arm. The ratio between the damping resistor of the high-voltage arm and the impedance of the low-voltage arm should be kept identical to the designed scale factor. This resistor is called the compensation resistor, and the degree of compensation p is defined as [28]

$$P = \frac{R_2 C_2}{RC} \tag{7}$$

The amplitude–frequency response curve of the voltage divider under different degrees of compensation is shown in Figure 10 for when $L_1 C_1 > L_2 C_2$. The results show that the upper cut-off frequency can be limited by a too high or too low degree of compensation. Generally, the degree of compensation is slightly less than 1. In this paper, the degree of compensation degree is about 0.8.
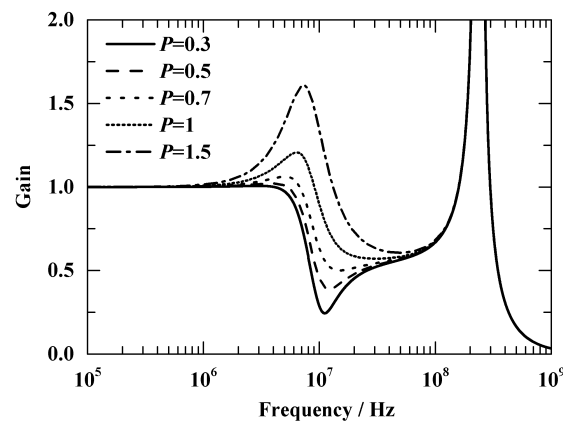
Figure 10. Amplitude–frequency characteristics with different degrees of compensation.

According to Figure 6, 40 groups of branches composed of a 22 nF capacitor and a 0.64 Ω resistor in series are connected in parallel at each side of the PCB. The branches at both sides are connected in series. The calculated capacitance of the low-voltage arm is 440 nF, and the compensation resistance of the low-voltage arm is 0.032 Ω. To limit the error of scale factors for DC, the power frequency and the lightning impulse within expectations, after calibration, it was determined that the parallel resistance in the low-voltage arm is composed of three 91 kΩ resistors in parallel and three 62 kΩ resistors in parallel at each side, and the series connection is arranged between two sides. Thus, the low-voltage arm has a parallel resistance of 24.58 kΩ.

5. Performance Test

5.1. Test Rig

The withstand voltage and scale factor of the developed voltage divider were tested by the DC source, power frequency transformer, lightning impulse generator and incidental standard voltage divider from Xi'an High Voltage Apparatus Research Institute Co., Ltd (Xi'an, China).

The step response evaluates the high-frequency performance of the measurement devices in the time domain [29,30]. The step response characteristics of the voltage divider were tested by a step voltage generator based on a mercury run switch. The open-circuit output voltage waveform is shown in Figure 11. The 10–90% rise time is about 3 ns.
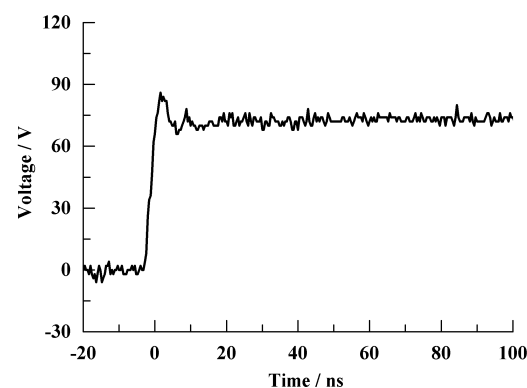
Figure 11. Output of the step voltage generator.

The frequency sweeping method was used to test the amplitude–frequency response of the voltage divider. The source includes a function generator and a broadband power amplifier. The function generator outputs a sinusoidal signal with an amplitude of ±5 V and a frequency range from DC ~20 MHz, which is increased to 35 V through the power amplifier and applied to the high-voltage terminal of the voltage divider. The test circuit

is shown in Figure 12. In the frequency sweeping test, 33 frequency points were sampled between 1 Hz and 15 MHz. Under each frequency, the ratio of the output signal of the voltage divider and the output of the standard high-voltage probe was recorded to obtain the amplitude–frequency response curve of the voltage divider.
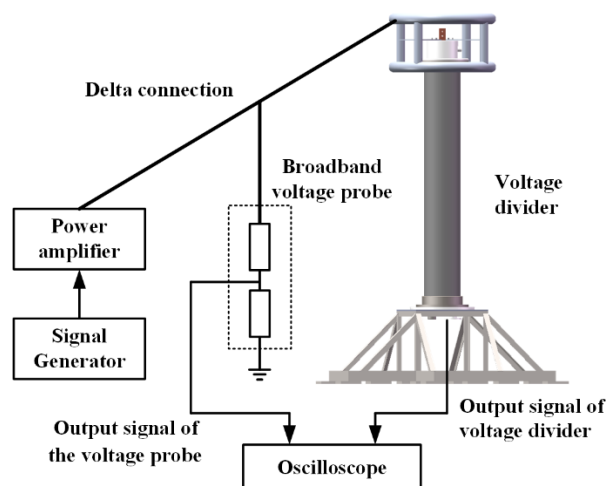
Figure 12. Schematic diagram of amplitude–frequency response test.

Because the voltage level is relatively low for the step response test and amplitude–frequency response test, a Tektronix tpp1000 passive voltage probe was used as the standard device.

5.2. Calibration of Insulation Strength and Scale Factor

The insulation withstand test and scale factor test were conducted under DC, a power frequency and a lightning impulse. No flashover or breakdown was found after one minute of a 360 kV power frequency voltage withstand test, a 200 kV DC voltage withstand test and 15 times positive and negative 1050 kV lightning impulses.

The scale factors under DC, the power frequency and the lightning impulse are shown in Tables 2–4. During the test, five groups of data at each test voltage were recorded, and the average values were computed. The scale factors under three types of voltages and different voltage levels are summarized in Figure 13. The test results show that when the scale factor of the voltage divider is calibrated to 10,500:1, the deviation is no more than 3% in measuring a DC voltage below 200 kV, a power frequency voltage below 220 kV and a lightning impulse below 700 kV. In the DC and power frequency voltage test, with the increase in the voltage, the temperature effects of the low-voltage arm components led to a certain decrease in the scale factor, but the change was so small that the overall linearity was still good.

Table 2. DC test results at room temperature.

Standard Device Output/kV	Divider Output/V	Scale Factor
49.929	4.8062	10,388
101.37	9.8091	10,335
152.42	14.921	10,215
203.53	19.964	10,195

Table 3. AC test results at room temperature.

Standard Device Output/kV	Divider Output/V	Scale Factor
49.721	4.6990	10,581
99.547	9.4464	10,538
148.78	14.132	10,528
218.34	20.789	10,503

Table 4. Lightning test results at room temperature.

Standard Device Output			Divider Output			Scale Factor
Peak/kV	Front Time/μs	Half-Width Time/μs	Peak/kV	Front Time/μs	Half-Width Time/μs	
217.9	1.53	46.2	207.7	1.48	44.6	10,491
385.4	1.51	46.4	367.8	1.44	45.2	10,479
501.9	1.52	46.4	473.6	1.4	46.2	10,598
629.8	1.53	46.6	598.8	1.43	46.6	10,518
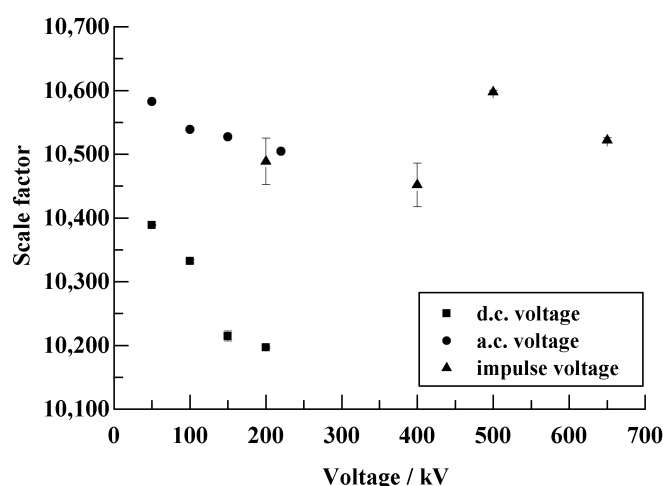
Figure 13. Test results of DC, power frequency and lightning impact voltage ratio at room temperature.

5.3. Temperature Stability

The temperature stability test was conducted with a scale factor test at the temperature of −20 °C or 40 °C, which was generated in a large artificial environment chamber. The results are summarized in Tables 5 and 6.

Table 5. Test results at −20 °C.

	Standard Device Output/kV	Divider Output/V	Scale Factor
DC	50.326	4.7889	10,509
	100.95	9.6151	10,499
	150.86	14.521	10,389
	200.55	19.309	10,386
Power Frequency	49.638	4.6214	10,741
	99.620	9.2894	10,724
	148.83	13.863	10,736
	218.76	20.393	10,727

Table 6. Test results at 40 °C.

	Standard Device Output/kV	Divider Output/V	Scale Factor
DC	55.352	5.2021	10,640
	107.29	10.081	10,643
	156.63	14.736	10,629
	204.85	19.454	10,530
Power Frequency	49.883	4.6381	10,755
	100.06	9.3180	10,738
	149.17	13.891	10,739
	219.59	20.457	10,734

The deviation between the scale factors at two extreme temperatures against the room temperature is no more than 3%; thus, the temperature stability of the voltage divider is good.

5.4. Step Response and Amplitude–Frequency Response

The output of the voltage divider is shown in Figure 14 for the wave response test. The output waveform is relatively flat, and the 10–90% rise time is about 29 ns. According to the mathematical relationship between the 10–90% rise time and the upper cut-off frequency [31,32]:

$$f_{\text{upper}} = \frac{0.35}{t_r} \tag{8}$$

the upper cut-off frequency of the divider is 12.2 MHz.
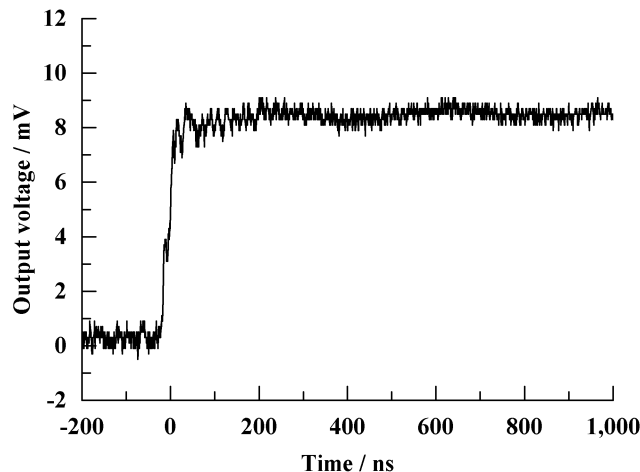
Figure 14. Step response waveform of the divider.

The amplitude–frequency response of the voltage divider obtained by the frequency sweeping method is shown in Figure 15. The experimental results show that the amplitude–frequency response is relatively flat in the low-frequency band as well as in the medium-frequency band. In the high-frequency band, the amplitude response rises slightly and then decreases afterwards. After calibration to a 50 Hz scale factor, a −3 dB point is found between 11 and 12 MHz, which matches 12.2 MHz as the time domain estimation. Therefore, the 3 dB upper cut-off frequency of the developed voltage divider exceeds 10 MHz.
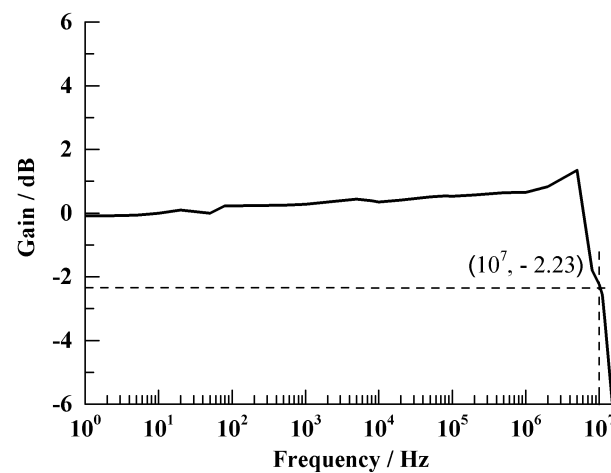
Figure 15. Amplitude–frequency characteristic curve of the divider.

6. Conclusions

In this paper, a broadband resistive–capacitive parallel-connected voltage divider for transient voltage monitoring of a 220 kV power grid was developed. The main conclusions are as follows:

(1) The internal electric field distribution of the voltage divider was optimized by using the structure of multi-stage series and multi-layer electrode plate shielding. The inductance of the high-voltage arm was reduced by adopting the circuit topology of multi-branch parallel connection, thus optimizing the response of the voltage divider.

(2) The factors affecting the upper cut-off frequency were analyzed, and a method to increase the upper cut-off frequency was proposed based on the compensation resistor of the low-voltage arm.

(3) The voltage divider meets the insulation requirements of high-voltage equipment, and the calibrated factor is 10,500:1. In the temperature range of −20~40 °C, the scale factor deviation is within 3% for measuring a DC voltage below 200 kV, a power frequency voltage below 220 kV and a lightning impulse below 700 kV.

(4) For the step response, the rise time is about 29 ns, and the 3 dB bandwidth covers DC to 10 MHz.

References

1. Du, L.; Li, X.; Sima, W.X.; Xi, S.Y.; Yang, Q.; Yuan, T. Overvoltage On-line Monitoring System for 110 kV Substation and Its Waveform Analysis. *High Volt. Eng.* **2012**, *38*, 535–543.
2. Zhou, X.; Qiu, Y.F.; Li, Z.J.; Miao, J. Transient Overvoltage On-line Monitoring Technology's Today and Tomorrow. In Proceedings of the 2015 Annual Conference of CSEE, Wuhan, China, 17–20 November 2015.
3. Zhang, C.Y.; Tang, S.; Liang, G.S.; Sun, H.F.; Wang, T.; Huang, T.; Ren, Y.Y. On-line Over-voltage Monitoring Method on Transmission Patameters of Voltage Transformer. In Proceedings of the 2011 Annual Conference of CSEE, Guiyang, China, 27–29 November 2011.
4. Ming, Z.Q. Study on Overvoltage On-line Monitoring System of High-Voltage Network. Master's Thesis, Chongqing University, Chongqing, China, 2008.
5. Wang, Y.Q.; Xie, J.; Lv, F.C.; Li, M.; Yan, C.Y.; Bi, J.G.; Yuan, S. An Overvoltage Method Based on Composite Integral Rogowski Coil. *Power Syst. Technol.* **2015**, *39*, 1450–1455.

6. Qiu, H.H. Investigations on the Key Technology and Relevant Theory of Electronic Transformers. Master's Thesis, Dalian University of Technology, Dalian, China, 2008.

7. Zhang, C.Y.; Li, W.B.; Chen, T. Online over-voltage monitoring algorithm based on broadband parameters of TV. *High Volt. Eng.* **2014**, *40*, 801–807. [CrossRef]

8. Liu, B.; Ren, L.; Xu, X.H.; Yang, W.H.; Xu, Y. On-line over-voltage monitoring system based on virtual instrument. *Electr. Power Autom. Equip.* **2007**, *27*, 97–100.

9. Pan, F.; Mu, Z.; Liu, H.; Wang, T.T.; Jiang, B.; Zhang, Y.; Zhang, C.M.; Xie, S.J.; Lin, G.S. Broadband Transient Model of CVT Based on Two-port Scaterring Parameters. *Sichuan Electr. Power Technol. Volt.* **2021**, *44*, 11–15. [CrossRef]

10. Li, W. Research on Electronic Current Transformer and New Technology Applied in Digital Power Station. Master's Thesis, Huazhong University of Science and Technology, Wuhan, China, 2011.

11. Jiang, Y.H. Designation and Research on the Methods of Online Monitoring Divider of Overhead Transmission Line. Master's Thesis, Xihua University, Chengdu, China, 2015.

12. Kovacevic, U.D.; Stankovic, K.D.; Kartalovic, N.M.; Loncar, B.B. Design of capacitive voltage divider for measuring ultrafast voltages. *Int. J. Electr. Power Energy Syst.* **2018**, *99*, 426–433. [CrossRef]

13. Brady, M.M.; Dedrick, K.G. High-Voltage Pulse Measurement with a Precision Capacitive Voltage Divider. *Rev. Sci. Instrum.* **1962**, *22*, 1421–1428. [CrossRef]

14. Thomas, R.J. High-Impulse Current and Voltage Measurement. *IEEE Trans. Instrum. Meas.* **1970**, *19*, 102–117. [CrossRef]

15. Hu, H.H. Study on Impulse Characteristics of Metallic Film Resistor and High-performance Resistive Divider. Master's Thesis, Huazhong University of Science and Technology, Wuhan, China, 1989.

16. Xie, S.J.; Zhang, C.M.; Ding, W.D.; Mei, K.S.; Han, X.Y.; Zhang, Y. Development and Uncertainty Evaluation of Sub-nanosecond Coaxial Resistive Divider. *High Volt. Eng.* **2020**, *46*, 4391–4399. [CrossRef]

17. Liu, Y.; Lin, F.C.; Hu, G.; Zhang, M. Design and Performance of a Resistive-Divider System for Measuring Fast HV Impulse. *IEEE Trans. Instrum. Meas.* **2011**, *60*, 996–1002. [CrossRef]

18. Harada, T.; Aoshima, Y.; Okamura, T.; Hiwa, K. Development of a high voltage universal divider. *IEEE Trans. Power Appar. Syst.* **1976**, *95*, 595–602. [CrossRef]

19. Hällström, J.; Bergman, A.; Dedeoğ, L.S.; Elg, A.P.; Houtzager, E.; Klüss, J.; Lehtonen, T.; Lucas, W.; Meisner, J.; Merev, A.; et al. Performance of a Modular Wideband HVDC Reference Divider for Voltages up to 1000 kV. *IEEE Trans. Instrum. Meas.* **2015**, *64*, 1390–1397. [CrossRef]

20. Zhou, K.; Zhang, T.; Dong, X.C.; Zhang, B.D.; Wang, J. Development of resistance-capacity divider for overvoltage online monitoring in distribution network. *Electrotech. Appl.* **2007**, *26*, 96–99.

21. Tang, N.P.; Rou, S.Y.; Liao, F.W. Research on High-voltage Measurement Device based on Space Electric Field. *Advaned Technol. Electr. Eng. Energy* **2009**, *29*, 25–28. [CrossRef]

22. Du, L.; Chang, A.F.; Sima, W.X.; Wang, Y.Y.; Lu, G.J. A non-contact overhead transmission line overvoltage sensor. *Autom. Electr. Power Syst.* **2010**, *34*, 93–97.

23. Dong, C.F.; Xiong, Z.Z.; Xie, S.J.; Zheng, L.Q.; Wang, R.H.; Xiang, J. Research on Measuring Device for Wideband Transient Electric Field. *Sichuan Electr. Power Technol. Volt.* **2020**, *43*, 12–16. [CrossRef]

24. Murase, H.; Okubo, H.; Aoyagi, H.; Yanabu, S. Development of 1-GHz GIS surge sensor. *Electr. Eng. Jpn.* **1989**, *109*, 32–38. [CrossRef]

25. Hao, H. A NPO Capacitive Dialectical Material and Its Preparation Method: China. Patent 110171965 A, 27 August 2019.

26. Ke, Y.G.; Cai, M.Y.; Zhao, H.Y.; Zhang, G.B.; Yang, W.; Tian, Y.; Zhu, T.Y. 3D Electric Field Simulation and Optimization of 40.5 kV Contact Box with Double Shield Structure. *High Volt. Appar.* **2020**, *56*, 23–28. [CrossRef]

27. Wang, J.C.; Ding, W.D.; Qiu, A.C. Capacitive sensor for fast pulsed voltage monitor in transmission line. *Rev. Sci. Instrum.* **2019**, *90*, 035107. [CrossRef] [PubMed]

28. Zhang, R.Y.; Chen, C.Y.; Wang, C.Z. *High-Voltage Testing Technology*; Tsinghua University Press: Beijing, China, 2009; ISBN 9787302204558.

29. Xie, S.J.; Mu, Z.; Ding, W.D.; Wang, J.C.; Su, F.F.; Liu, Y. Development of the 100kV Square Wave Generator with Nanosecond Rise Time. *High Volt. Eng.* **2021**, *47*, 2169–2176. [CrossRef]

30. Su, S.C.; Xie, S.J.; Ding, W.D.; Liu, Y.; Yan, J.Y.; Mu, Z. Development of 2 kV Square Wave Source with Sub-nanosecond Rise Time Using for the Calibration of VFTO Sensors. *High Volt. Eng.* **2020**, *46*, 2976–2983. [CrossRef]

31. Yue, G.C.; Liu, W.D.; Chen, W.J.; Guan, Y.G.; Li, Z.B. Calibration of Very Fast Transient Overvoltage Measurement System for Ultra High Voltage Gas Insulated Switchgear. *High Volt. Eng.* **2012**, *38*, 342–349.

32. Zeng, C. Relation between -3 dB frequency and risetime for resistive voltage divider. *High Power Laser Part. Beans* **2005**, *17*, 1065–1069.